AE370 Group Project 2

Aditi Badde, Kulvir Chavda, Ayush Gupta, Aadyanth Rao, Ram Velamuri

14th May, 2025

1 Presenting an IBVP relevant to engineering

1.1 A Relevant Engineering IBVP and Its Importance

The initial boundary value problem (IBVP) we examine in this project is the **one-dimensional linear convection-diffusion equation**:

$$\frac{\partial u}{\partial t} + v\frac{\partial u}{\partial x} = D\frac{\partial^2 u}{\partial x^2}, \quad x \in [a, b], \quad t > 0$$

where:

- $u(x, t)$ represents the transported quantity (e.g., temperature, concentration),

- v is the constant convection (advection) velocity,

- D is the diffusion coefficient (assumed constant),

- $[a, b]$ is the spatial domain of interest.

This equation is highly relevant in many branches of engineering because it captures the combined physics of **advection** (which transports the quantity downstream with the flow) and **diffusion** (which smooths out gradients due to molecular mixing or random motion). Its importance stems from its widespread appearance in modeling transport phenomena across disciplines:

- **Mechanical and Aerospace Engineering:** modeling of heat transfer in boundary layers, flow of gases or plasma in ducts, and cooling of electronic components.

- **Environmental Engineering:** predicting the dispersion of pollutants in rivers or the atmosphere.

- **Chemical Engineering:** describing the transport of reactants or heat in chemical reactors or catalytic converters.

- **Biomedical Engineering:** modeling drug diffusion and transport in blood vessels or tissue under flow conditions.

The convection-diffusion IBVP is also compelling from a numerical standpoint. The presence of both **first-order** and **second-order** spatial derivatives leads to layered behavior, such as *boundary layers* or *sharp fronts*, depending on the relative strength of v and D. When convection dominates ($v \gg D$), the problem becomes *advection-dominated*, and standard numerical methods may develop spurious oscillations or numerical diffusion unless appropriately stabilized.

This makes the problem ideal for:

- Evaluating the **accuracy, stability, and convergence** of numerical schemes,

- Studying the influence of the **Péclet number** $Pe = \frac{v(b-a)}{D}$,

- Designing **robust discretizations** that resolve steep gradients without sacrificing stability or accuracy.

Ultimately, this equation bridges mathematical theory with practical engineering modeling and computational implementation—making it both ambitious and feasible for systematic numerical investigation.

1.2 Questions to Explore with the Convection–Diffusion IBVP

We will sweep
$$Pe = \{0.1,\ 1,\ 10,\ 100,\ 1000\}$$
to span diffusion-dominated ($Pe \ll 1$), mixed ($Pe \approx 1$), and advection-dominated ($Pe \gg 1$) regimes.

A. Boundary-layer Thickness & Front Speed vs. Pe

For each $Pe \in \{0.1,\ 1,\ 10,\ 100,\ 1000\}$, we compute the transient solution $u(x,t)$ up to a fixed time t_1.

- **Measure** the boundary-layer thickness δ_{Pe} at t_1 as the distance over which u drops from $0.9\,u_{\max}$ to $0.1\,u_{\max}$.

- **Compute** the front propagation speed:

$$s_{Pe} = \frac{d\,x_{\text{front}}}{dt}.$$

Question: How do δ_{Pe} and s_{Pe} scale with Pe?

B. Accuracy & Stability: FDM vs. FEM

Using $\Delta x = (b-a)/N$ with $N \in \{50,\ 100,\ 200\}$ and Crank–Nicolson time integration:

- **Time-step choice:** no CFL-type limit, so choose

$$\Delta t \approx \Delta x$$

  to balance $\mathcal{O}(\Delta x^2)$ spatial error with $\mathcal{O}(\Delta t^2)$ temporal error.

- **Manufactured solution:**
$$u_{\text{ex}}(x,t) = e^{-t}\,\sin(\pi x)$$
  with appropriate forcing to compute L^2 errors.

- **FDM:** second-order central differences in space.

- **FEM:** Galerkin with continuous piecewise-linear "hat" basis.

Question: For each Pe and Δx, what is the L^2 error at t_1? At which Pe does FDM first exhibit nonphysical oscillations compared to FEM?

C. Convergence Study: Δx and Δt Requirements

Fix $Pe \in \{1,\ 100\}$:

- Vary $\Delta x \in \left\{ \frac{1}{50},\ \frac{1}{100},\ \frac{1}{200} \right\}$; choose

$$\Delta t \text{ such that } \frac{v\,\Delta t}{\Delta x} = 0.5.$$

  (Alternatively, $\Delta t = \mathcal{O}(\Delta x^2)$ ensures $\mathcal{O}(\Delta x^4)$ temporal error to isolate spatial convergence.)

- Compute L^2 error at t_1 vs. the manufactured solution.

Question: Do we observe second-order spatial convergence (error $\propto \Delta x^2$) and first-order temporal convergence (error $\propto \Delta t$)? What resolution is needed for L^2-error $\leq 10^{-3}$ at $Pe = 100$?

D. Method Comparison: FDM vs. FEM Trade-Offs

For $Pe \in \{10, 100, 1000\}$ on a fixed grid ($\Delta x = 1/100$, with Δt satisfying $v\,\Delta t / \Delta x = 0.5$), compare:

1. FDM + Crank–Nicolson

2. FEM + Crank–Nicolson

Question: Which method yields lower oscillations and smaller L^2 error at t_1? What is the trade-off in CPU time vs. accuracy?

By answering these questions, we build a robust understanding of convection-diffusion behavior across regimes, how time-stepping affects error balance, and when standard schemes break down—guiding solver selection and stabilization in practical simulations.

1.3 Mathematical Formulation of the Convection–Diffusion IBVP

A. Continuous IBVP

Governing PDE (strong form):

$$\frac{\partial u}{\partial t} + v\,\frac{\partial u}{\partial x} = D\,\frac{\partial^2 u}{\partial x^2}, \quad x \in (0,1),\ t \in (0,T].$$

Initial condition:

$$u(x,0) = h(x) = \exp\left(-\frac{(x-0.5)^2}{2\sigma^2}\right), \quad \sigma = 0.1.$$

Boundary conditions (homogeneous Dirichlet):

$$u(0,t) = 0, \quad u(1,t) = 0, \quad t \in [0,T].$$

B. Finite-Difference (Method-of-Lines) Formulation

1. **Spatial grid:**
$$x_j = j\,\Delta x, \quad j = 0,\ldots,n+1, \quad \Delta x = \frac{1}{n+1}.$$

   Unknowns:
$$u_j^n \approx u(x_j, t^n), \quad j = 1,\ldots,n, \quad u_0^n = u_{n+1}^n = 0.$$

2. **Second-order centered derivatives:**
$$\left.\frac{\partial u}{\partial x}\right|_{x_j} \approx \frac{u_{j+1} - u_{j-1}}{2\,\Delta x}, \quad \left.\frac{\partial^2 u}{\partial x^2}\right|_{x_j} \approx \frac{u_{j+1} - 2u_j + u_{j-1}}{\Delta x^2}.$$

3. **Semi-discrete ODE system:**
$$\dot{u}_j(t) = -v\,\frac{u_{j+1} - u_{j-1}}{2\,\Delta x} + D\,\frac{u_{j+1} - 2u_j + u_{j-1}}{\Delta x^2}, \quad j = 1,\ldots,n.$$

4. **Time integration (Crank–Nicolson):**
$$u^{n+1} = u^n + \frac{\Delta t}{2}\left(f(u^n, t^n) + f(u^{n+1}, t^{n+1})\right),$$

   where $f(u,t)$ is the spatial right-hand side. In matrix form:
$$\left(I - \frac{\Delta t}{2}A\right)u^{n+1} = \left(I + \frac{\Delta t}{2}A\right)u^n,$$

   with A the FDM discretization matrix.

C. Finite-Element (Galerkin) Formulation

1. **Mesh & basis:** Partition $[0, 1]$ into $N+1$ equal subintervals of length Δx. Let $\{\phi_i(x)\}_{i=1}^N$ be piecewise-linear "hat" functions vanishing at $x = 0, 1$.

2. **Weak form:** Find $u_h(t) \in V_h = \text{span}\{\phi_i\}$ such that for each test ϕ_j:

$$\int_0^1 \phi_j \frac{\partial u_h}{\partial t} \, dx + v \int_0^1 \phi_j \frac{\partial u_h}{\partial x} \, dx + D \int_0^1 \phi_j' \frac{\partial u_h}{\partial x} \, dx = 0.$$

3. **Matrix assembly:**

$$M_{ij} = \int_0^1 \phi_i \, \phi_j \, dx, \quad C_{ij} = \int_0^1 \phi_i \, \phi_j' \, dx, \quad K_{ij} = \int_0^1 \phi_i' \, \phi_j' \, dx.$$

Semi-discrete system:

$$M \dot{U}(t) + v \, C \, U(t) + D \, K \, U(t) = 0, \quad U(t) = [u_1(t), \dots, u_N(t)]^\top.$$

4. **Time stepping (Crank–Nicolson):**

$$\left(M + \frac{\Delta t}{2}(v \, C + D \, K) \right) U^{n+1} = \left(M - \frac{\Delta t}{2}(v \, C + D \, K) \right) U^n.$$

D. Parameters & Discretization Settings

- **Physical parameters:**

$$v \in \{0.1, 1, 10\}, \quad D \in \{0.01, 0.1, 1\}, \quad T = 0.5 \Rightarrow Pe = \frac{v}{D} \in \{0.1, 1, 10, 100, 1000\}.$$

- **Spatial discretization:**

$$\Delta x \in \left\{ \frac{1}{40}, \frac{1}{80}, \frac{1}{160} \right\}.$$

- **Temporal discretization:**

  - **FDM:** choose Δt such that $v \, \Delta t / \Delta x = 0.5$.
  - **FEM:** no explicit stability limit (implicit method); choose Δt comparable to FDM for fair CPU-accuracy comparison.

2 Presenting an appropriate numerical method to study the dynamical system

2.1 Justification: Accuracy, Stability, and Cost Considerations

We adopt the Crank–Nicolson (trapezoidal) method for time integration, combined with two spatial discretizations: second-order finite differences (FDM) and continuous piecewise-linear finite elements (FEM). The following considerations justify this choice:

- **Accuracy:**

  FDM with second-order centered differences in space yields formal error

$$\|u - u_h\| = \mathcal{O}(\Delta x^2).$$

  FEM with continuous piecewise-linear "hat" basis also delivers

$$\|u - u_h\| = \mathcal{O}(\Delta x^2).$$

- **Stability:**

  The semi-discrete diffusive operator has eigenvalues scaling like $D/\Delta x^2$, making the ODE stiff.

  Crank–Nicolson (trapezoidal) is A-stable and second-order in time ($\mathcal{O}(\Delta t^2)$), so we can choose Δt based on accuracy (e.g. $\Delta t \approx \Delta x$ or $\Delta t \approx \Delta x^2$) rather than a stability limit.

- **Cost:**

  Each time step requires solving one sparse linear system:
  - **FDM:** tridiagonal matrix $\Rightarrow \mathcal{O}(n)$ solve.
  - **FEM:** sparse banded mass+stiffness $\Rightarrow \mathcal{O}(n)$–$\mathcal{O}(n \log n)$ solve in practice.

  This low per-step cost makes it feasible to sweep over many Pe, Δx, and Δt configurations.

2.2 Mathematical Derivation of FDM and FEM Schemes

A. Finite-Difference Discretization

1. General p-point interpolation

Approximate $u(x,t)$ near x_j by a degree-p polynomial through $\{x_{j-m}, \ldots, x_{j+m}\}$, where $p = 2m$ or $2m+1$:

$$u(x,t) \approx \sum_{k=-m}^{m} u_{j+k}(t)\, L_{j+k}^{(p)}(x),$$

with $L_{j+k}^{(p)}(x)$ the Lagrange basis polynomial satisfying $L_{j+k}^{(p)}(x_{j+\ell}) = \delta_{k\ell}$.

Differentiating at x_j gives:

$$\left.\frac{\partial u}{\partial x}\right|_{x_j} \approx \sum_{k=-m}^{m} u_{j+k} \left(L_{j+k}^{(p)}\right)'(x_j), \quad \left.\frac{\partial^2 u}{\partial x^2}\right|_{x_j} \approx \sum_{k=-m}^{m} u_{j+k} \left(L_{j+k}^{(p)}\right)''(x_j).$$

2. Special case $p = 2$ $(m = 1)$

Using nodes x_{j-1}, x_j, x_{j+1}:

$$\left(L_{j\pm1}^{(2)}\right)'(x_j) = \pm\frac{1}{2\Delta x}, \quad \left(L_j^{(2)}\right)'(x_j) = 0,$$

$$\left(L_{j-1}^{(2)}\right)''(x_j) = \frac{1}{\Delta x^2}, \quad \left(L_j^{(2)}\right)''(x_j) = -\frac{2}{\Delta x^2}, \quad \left(L_{j+1}^{(2)}\right)''(x_j) = \frac{1}{\Delta x^2}.$$

Hence,

$$\left.\frac{\partial u}{\partial x}\right|_{x_j} \approx \frac{u_{j+1} - u_{j-1}}{2\Delta x}, \quad \left.\frac{\partial^2 u}{\partial x^2}\right|_{x_j} \approx \frac{u_{j+1} - 2u_j + u_{j-1}}{\Delta x^2}.$$

3. Semi-discrete ODE system

Substitute into the PDE $u_t + v\, u_x = D\, u_{xx}$:

$$\frac{du_j}{dt} = -v\, \frac{u_{j+1} - u_{j-1}}{2\Delta x} + D\, \frac{u_{j+1} - 2u_j + u_{j-1}}{\Delta x^2}.$$

4. Consistency and truncation error

Taylor expand $u_{j\pm1}$ about x_j:

$$u_{j\pm1} = u_j \pm \Delta x\, u_x + \frac{\Delta x^2}{2}\, u_{xx} \pm \frac{\Delta x^3}{6}\, u_{xxx} + \mathcal{O}(\Delta x^4).$$

So,

$$\frac{u_{j+1} - u_{j-1}}{2\Delta x} = u_x + \mathcal{O}(\Delta x^2), \quad \frac{u_{j+1} - 2u_j + u_{j-1}}{\Delta x^2} = u_{xx} + \mathcal{O}(\Delta x^2).$$

Thus, spatial error is $\mathcal{O}(\Delta x^2)$.

5. Time integration and stability

Apply Crank–Nicolson:

$$u_j^{n+1} = u_j^n + \frac{\Delta t}{2} \left(f_j^n + f_j^{n+1} \right), \quad f_j = -v \frac{u_{j+1} - u_{j-1}}{2\Delta x} + D \frac{u_{j+1} - 2u_j + u_{j-1}}{\Delta x^2}.$$

Matrix form:

$$\left(I - \frac{\Delta t}{2} A \right) U^{n+1} = \left(I + \frac{\Delta t}{2} A \right) U^n.$$

Amplification factor for eigenvalue λ of A:

$$G(\lambda) = \frac{1 + \frac{\Delta t}{2}\lambda}{1 - \frac{\Delta t}{2}\lambda}, \quad \text{with } \Re(\lambda) \le 0 \Rightarrow |G(\lambda)| \le 1.$$

Conclusion: Crank–Nicolson is unconditionally stable (A-stable).

B. Finite-Element Discretization

1. General weighted-residual form

Find $u_h \in V_h$ such that for all $\phi \in V_h$:

$$\int_0^1 \phi \left(u_t + v\, u_x - D\, u_{xx} \right) dx = 0.$$

2. Weak form via integration by parts

Apply integration by parts to the diffusion term (with $\phi(0) = \phi(1) = 0$):

$$\int_0^1 \phi\, u_{xx}\, dx = -\int_0^1 \phi'\, u_x\, dx,$$

so the weak form becomes:

$$\int_0^1 \phi\, u_t\, dx + v \int_0^1 \phi\, u_x\, dx - D \int_0^1 \phi'\, u_x\, dx = 0.$$

3. Assembly of system matrices

Let $u_h(x,t) = \sum_{i=1}^N U_i(t)\, \phi_i(x)$. Then:

$$\sum_i \dot{U}_i \int_0^1 \phi_i\, \phi_j\, dx + v \sum_i U_i \int_0^1 \phi_i\, \phi_j'\, dx + D \sum_i U_i \int_0^1 \phi_i'\, \phi_j'\, dx = 0.$$

Define:

$$M_{ij} = \int_0^1 \phi_i\, \phi_j\, dx, \quad C_{ij} = \int_0^1 \phi_i\, \phi_j'\, dx, \quad K_{ij} = \int_0^1 \phi_i'\, \phi_j'\, dx.$$

4. Semi-discrete system and time stepping

The semi-discrete system is:

$$M\, \dot{U} + v\, C\, U + D\, K\, U = 0.$$

Apply Crank–Nicolson:

$$\left(M + \frac{\Delta t}{2}(v\, C + D\, K) \right) U^{n+1} = \left(M - \frac{\Delta t}{2}(v\, C + D\, K) \right) U^n.$$

Error: Spatial error is $\mathcal{O}(\Delta x^2)$, temporal error is $\mathcal{O}(\Delta t^2)$. An energy argument using symmetry of K and skew-symmetry of C shows stability in the discrete M-norm.

2.3 Algorithmic Summary: Advancing from t_k to t_{k+1}

Given physical parameters v, D, final time T, and discretization sizes N_x, N_t:

1. **Discretization**

   - $\Delta x = \dfrac{1}{N_x + 1}$

   - $\Delta t = \dfrac{T}{N_t}$

   - Spatial nodes $x_j = j\,\Delta x$ for $j = 0, 1, \ldots, N_x + 1$.

2. **Assemble spatial operators**

   - **FDM:** build the tridiagonal matrix A_{FDM} using the 3-point centered stencil

   $$(A_{\mathrm{FDM}})_{j,j-1} = \frac{D}{\Delta x^2} - \frac{v}{2\,\Delta x}, \quad (A_{\mathrm{FDM}})_{j,j} = -\frac{2D}{\Delta x^2}, \quad (A_{\mathrm{FDM}})_{j,j+1} = \frac{D}{\Delta x^2} + \frac{v}{2\,\Delta x}.$$

   - **FEM:** assemble

   $$M_{ij} = \int_0^1 \phi_i\,\phi_j\,dx, \quad C_{ij} = \int_0^1 \phi_i\,\phi_j'\,dx, \quad K_{ij} = \int_0^1 \phi_i'\,\phi_j'\,dx,$$

   using continuous piecewise-linear "hat" functions.

3. **Precompute time-stepping matrices**

   - Let I be the $N_x \times N_x$ identity.

   - **FDM:**

   $$L_{\mathrm{FDM}} = I - \frac{\Delta t}{2} A_{\mathrm{FDM}}, \qquad R_{\mathrm{FDM}} = I + \frac{\Delta t}{2} A_{\mathrm{FDM}}.$$

   - **FEM:**

   $$L_{\mathrm{FEM}} = M + \frac{\Delta t}{2}\,(v\,C + D\,K), \qquad R_{\mathrm{FEM}} = M - \frac{\Delta t}{2}\,(v\,C + D\,K).$$

   - Factorize L_{FDM} and L_{FEM} once for efficient solves.

4. **Initialize solutions at $t = 0$**

   - **FDM:**

   $$U^0_{\mathrm{FDM}}[j] = h(x_j) \quad \text{for } j = 1, \ldots, N_x, \quad \text{with boundaries } U^0_{\mathrm{FDM}}[0] = U^0_{\mathrm{FDM}}[N_x + 1] = 0.$$

   - **FEM:**

   $$U^0_{\mathrm{FEM}} = M^{-1} \left[\int_0^1 h(x)\,\phi_i(x)\,dx \right]_{i=1}^{N},$$

   or simply sample $h(x_j)$ and optionally lump the mass.

5. **Time-stepping loop**

   For $n = 0, 1, \ldots, N_t - 1$:

   $$L_{\mathrm{FDM}}\,U^{n+1}_{\mathrm{FDM}} = R_{\mathrm{FDM}}\,U^n_{\mathrm{FDM}}, \qquad L_{\mathrm{FEM}}\,U^{n+1}_{\mathrm{FEM}} = R_{\mathrm{FEM}}\,U^n_{\mathrm{FEM}}.$$

6. **Reconstruct and return**

   - Enforce Dirichlet BCs by prepending/appending zeros to each interior vector.
   - Return $(x,\, u_{\mathrm{FDM}}(T),\, u_{\mathrm{FEM}}(T))$.

3   Implementation and Convergence Studies

In the following solution to problem 3, we not only confirm the formal second-order accuracy of our Crank–Nicolson FDM and FEM schemes via a manufactured-solution test, but we also illustrate how the local cell Péclet number

$$Pe_{\text{cell}} = \frac{v\,\Delta x}{D}$$

governs whether that convergence is observed.

1. **Diffusion-Dominated Regime** ($Pe_{\text{cell}} < 2$)

   - Choose v and D so that $Pe_{\text{cell}} < 2$ (for example $v = 0.1$, $D = 1$).
   - **Time-step scaling:** set
     $$\Delta t = C\,\Delta x^2,$$
     in accordance with the diffusion-stability limit derived in Lecture 21. This makes the temporal truncation error $\mathcal{O}(\Delta x^4)$, so spatial error $\mathcal{O}(\Delta x^2)$ dominates and is cleanly observed.
   - Compute the L^2-error at $T = 0.5$

     $$E(N_x) = \left(\Delta x \sum_{j=1}^{N_x} \left(u_j^N - u_{\text{ex}}(x_j, T) \right)^2 \right)^{1/2}$$

     for FDM, and

     $$E(N_x) = \sqrt{(U^N - U_{\text{ex}})^T\, M\, (U^N - U_{\text{ex}})}$$

     for FEM, using $u_{\text{ex}}(x,t) = e^{-t}\sin(\pi x)$.
   - Produce log–log plots of E vs. Δx with an $\mathcal{O}(\Delta x^2)$ reference line. **Expected:** both methods show slope 2.

2. **Advection-Dominated Regime** ($Pe_{\text{cell}} > 2$)

   - Increase Pe_{cell} (e.g. $v = 1$, $D = 0.1$ gives $Pe_{\text{cell}} \approx 10$).
   - Repeat the convergence test on the same mesh sequence with $\Delta t = C\,\Delta x^2$.
   - **Observe:** errors plateau or oscillate instead of following the Δx^2 slope, revealing the breakdown of undamped central/Galerkin schemes at high Péclet numbers.

3. **Solution Snapshots**

   - For both regimes, plot numerical (blue markers) vs. exact (orange line) solutions on very coarse and fine meshes (e.g. $N_x = 3,\ 15,\ 50$) to visualize error behavior.

4. **Interpretation**

   - **Time-step assumption:** scaling $\Delta t \sim \Delta x^2$ comes from the physical diffusion timescale $\Delta t_{\text{diff}} \approx \Delta x^2/D$ and ensures stability and an error-balance that highlights spatial convergence.
   - **Péclet criterion:** when $Pe_{\text{cell}} < 2$, central differences and standard Galerkin FEM recover $\mathcal{O}(\Delta x^2)$ accuracy; once $Pe_{\text{cell}} > 2$, these undamped schemes fail to converge because the advective truncation error and dispersive instabilities dominate.
   - **Physical meaning:** choosing Δt on the order of the diffusion time across one cell ensures the numerical method resolves the physics of mixing on the grid scale without temporal error overwhelming spatial accuracy.

FDM Convergence (dt ~ dx^2)

FEM Convergence (dt ~ dx^2)
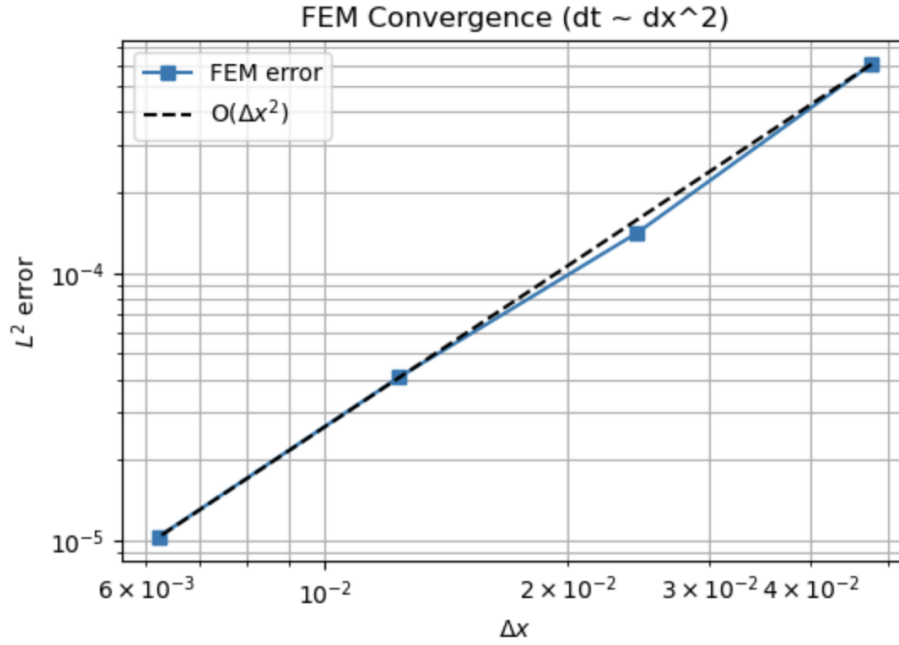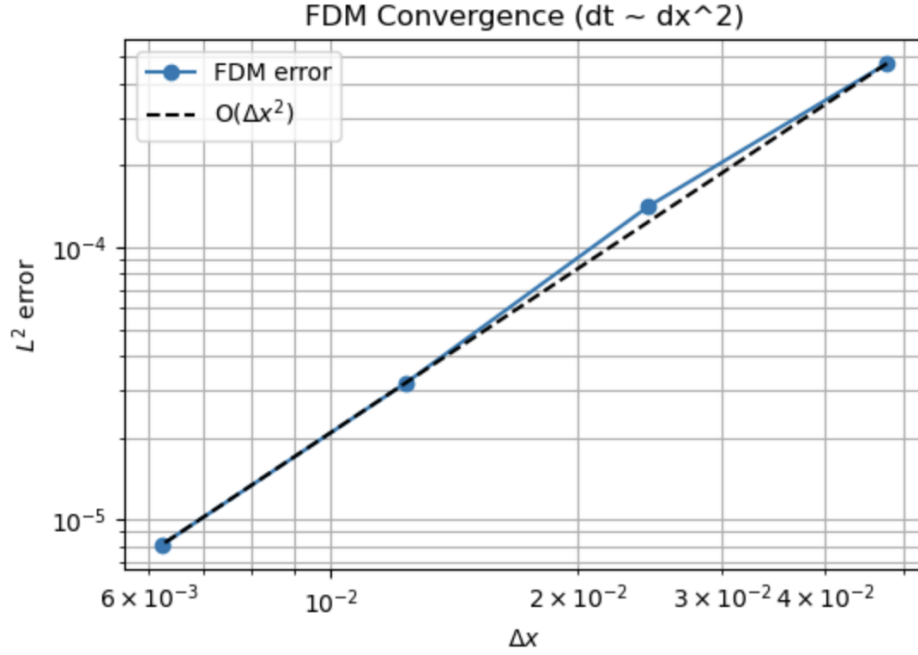
1. **Effect of Parabolic Time-Step Scaling**

   By choosing $\Delta t = C \, \Delta x^2$, we ensure the Crank–Nicolson temporal error is $\mathcal{O}(\Delta x^4)$, making it negligible compared to the spatial $\mathcal{O}(\Delta x^2)$ error. This clean separation causes the log–log convergence plots to align with the reference slope-2 line, clearly demonstrating second-order spatial accuracy.

   If instead we use $\Delta t = \Delta x$, then the temporal error $\mathcal{O}(\Delta t^2) = \mathcal{O}(\Delta x^2)$ is the same order as the spatial error. The resulting L^2 errors combine both contributions, and the log–log plots do *not* cleanly follow the $\mathcal{O}(\Delta x^2)$ reference—they flatten out, masking true spatial convergence.

9

FDM Convergence (dt = Δx)

FEM Convergence (dt = Δx)
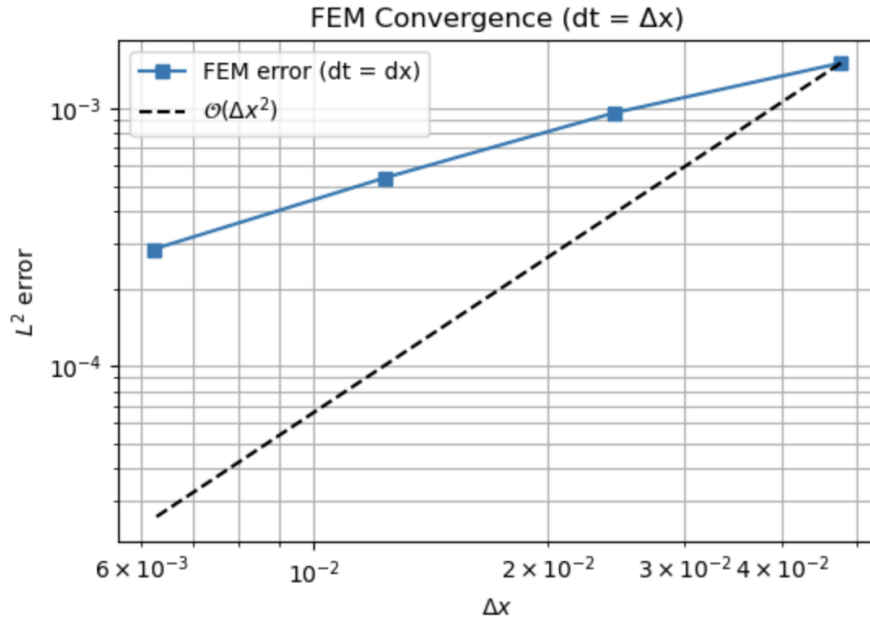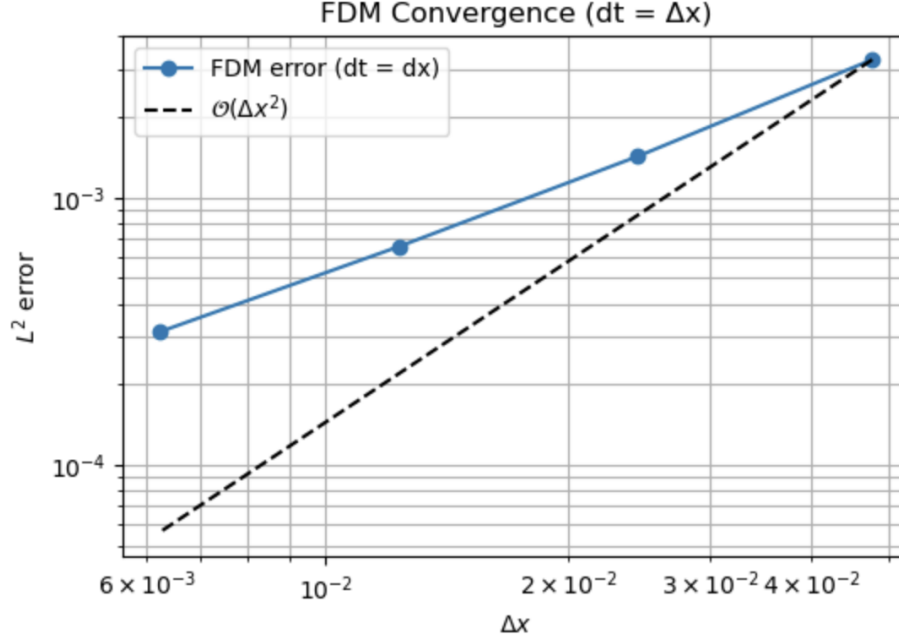
2. **Advection-Dominated Regime** $(Pe_{\text{cell}} > 2)$

- **Parameter choice:** set, for example,

$$v = 1, \quad D = 0.1 \quad \Longrightarrow \quad Pe_{\text{cell}} = \frac{v\,\Delta x}{D} \approx 10 \quad (\text{on } \Delta x \sim 0.1).$$

- **Mesh & time-step:** use the same $N_x \in \{20,\ 40,\ 80,\ 160\}$ and

$$\Delta t = C\,\Delta x^2$$

as in the diffusion-dominated study, so temporal error remains $\mathcal{O}(\Delta x^4)$.

- **Convergence test:** for each N_x, compute the discrete L^2 error at $t = T$ using the manufactured solution

$$u_{\text{ex}}(x, t) = e^{-t} \sin(\pi x)$$

with the corresponding forcing term, both for FDM (central-difference + Crank–Nicolson) and FEM (Galerkin + Crank–Nicolson).

- **Expected outcome:** because the cell-Péclet number now exceeds the stability threshold ($Pe_{\text{cell}} > 2$), neither the undamped central FDM nor the standard Galerkin FEM will recover the formal $\mathcal{O}(\Delta x^2)$ rate. On log–log plots of error vs. Δx, the curves will **flatten** or even **oscillate** instead of aligning with the slope-2 reference line, illustrating the breakdown of these schemes in advection-dominated flows.

- **Interpretation:** this failure occurs because central stencils (in both FDM and FEM) lack built-in upwinding or stabilization, so when advection dominates diffusion the leading truncation errors and dispersive instabilities no longer vanish at $\mathcal{O}(\Delta x^2)$.
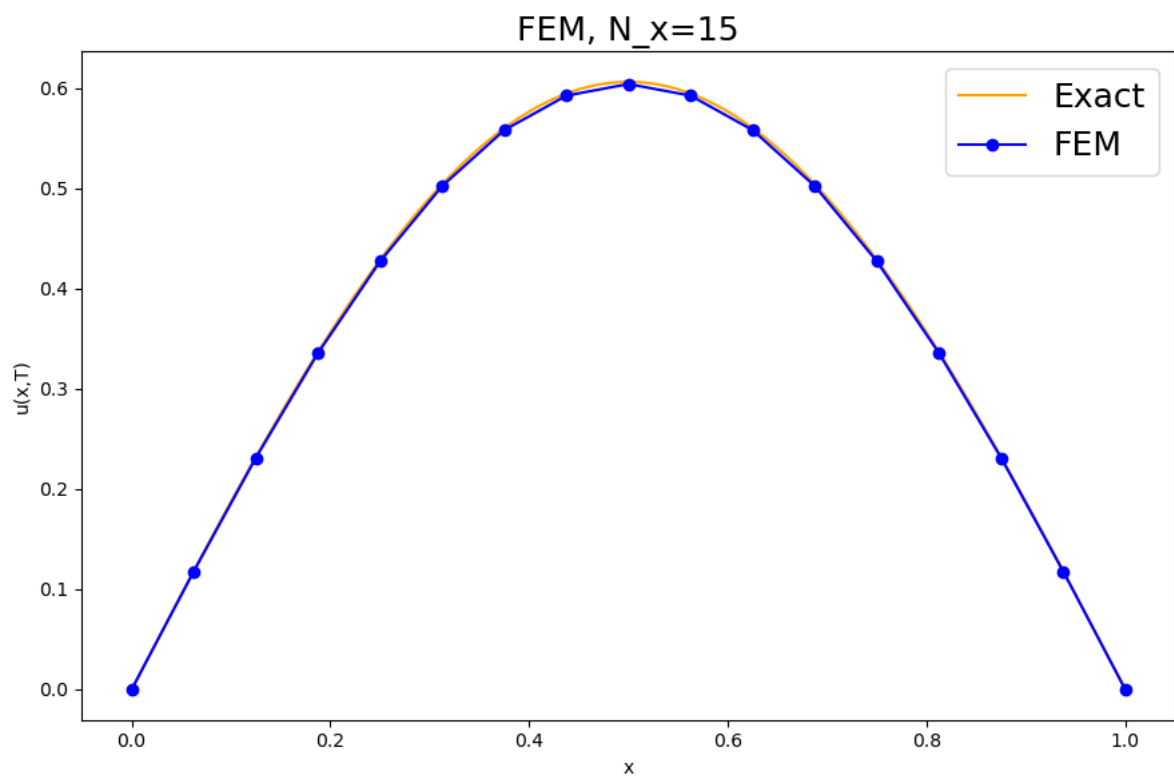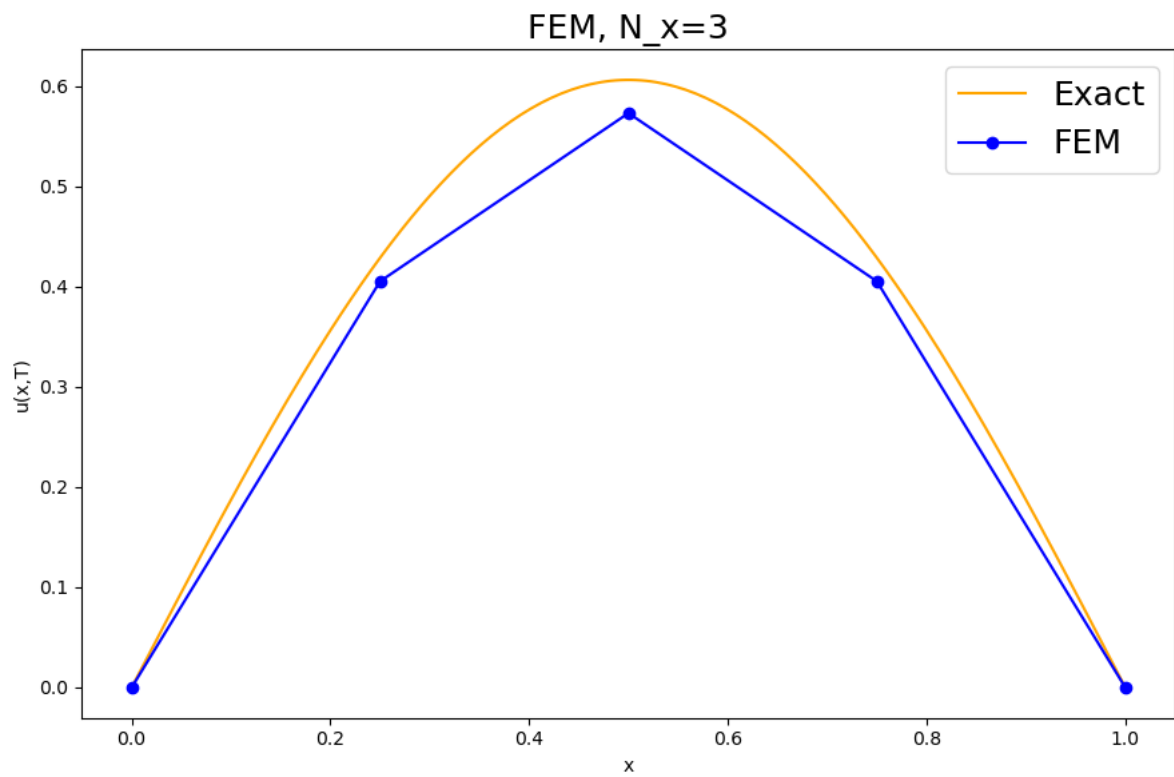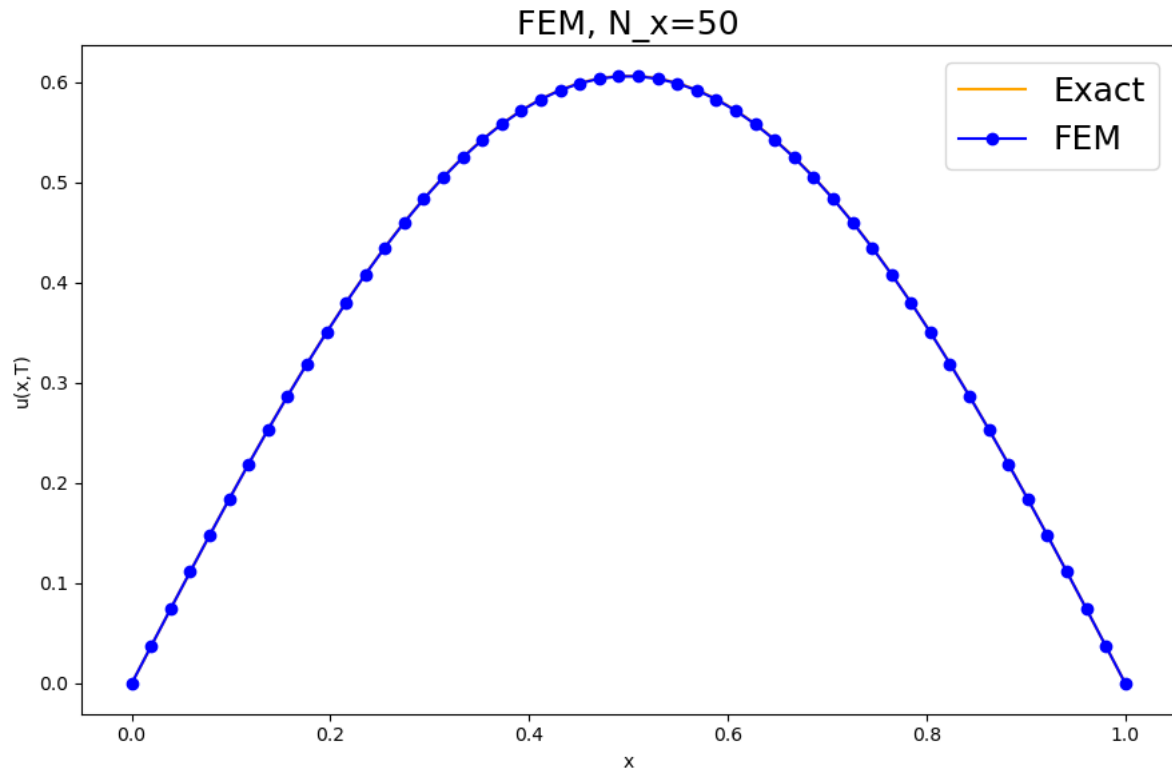
FEM Convergence ($Pe_{\text{cell}} \approx 10$)
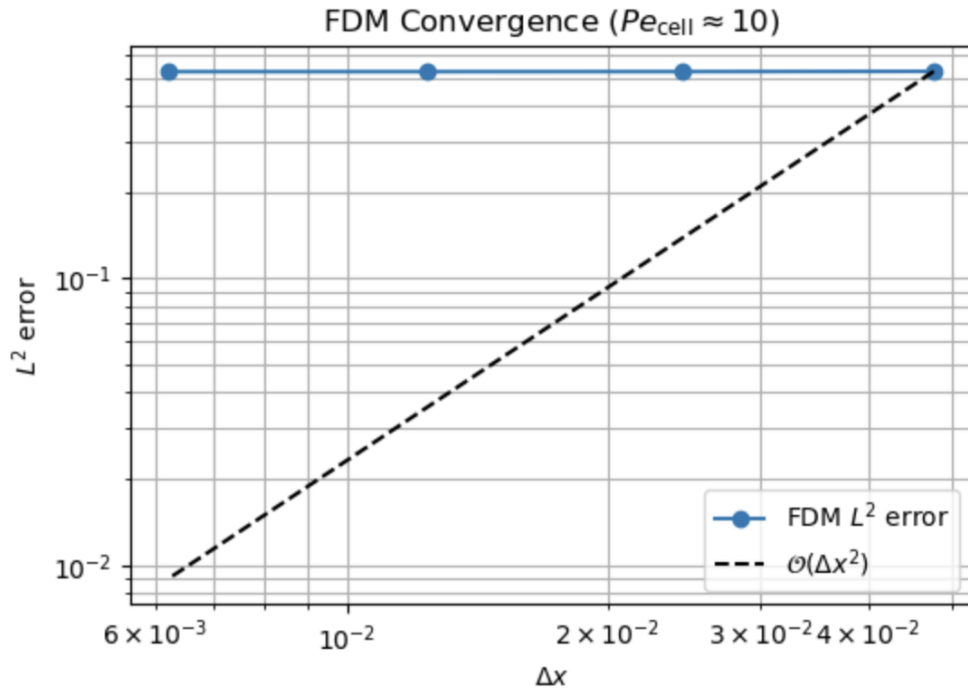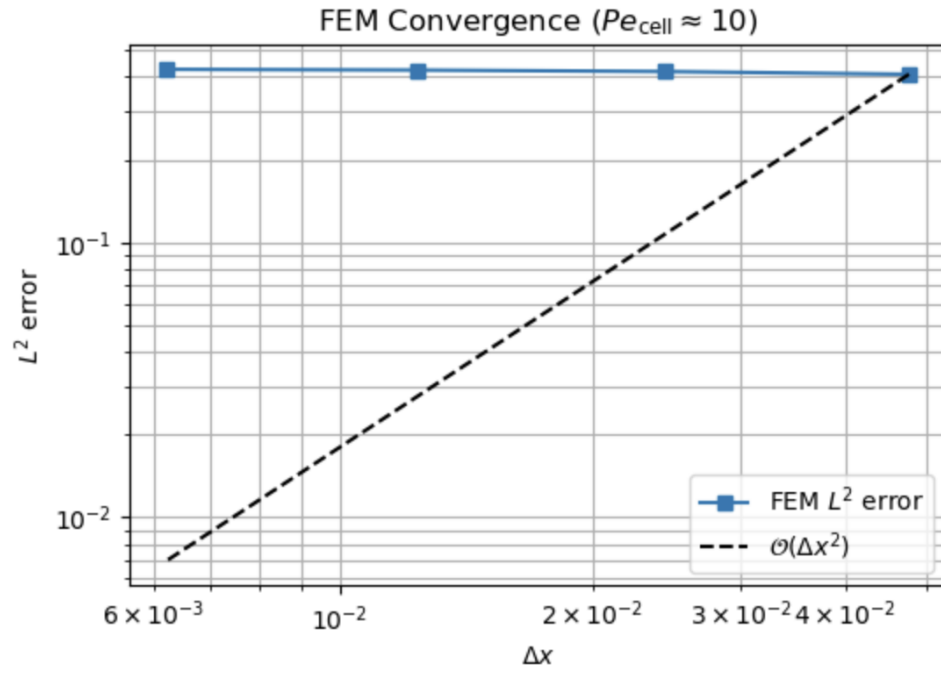
3. **Solution Snapshots**

- For both regimes, we plot numerical (blue markers) vs. exact (orange line) solutions on very coarse and fine meshes (e.g. $N_x = 3$, 15, 50) to visualize error behavior.
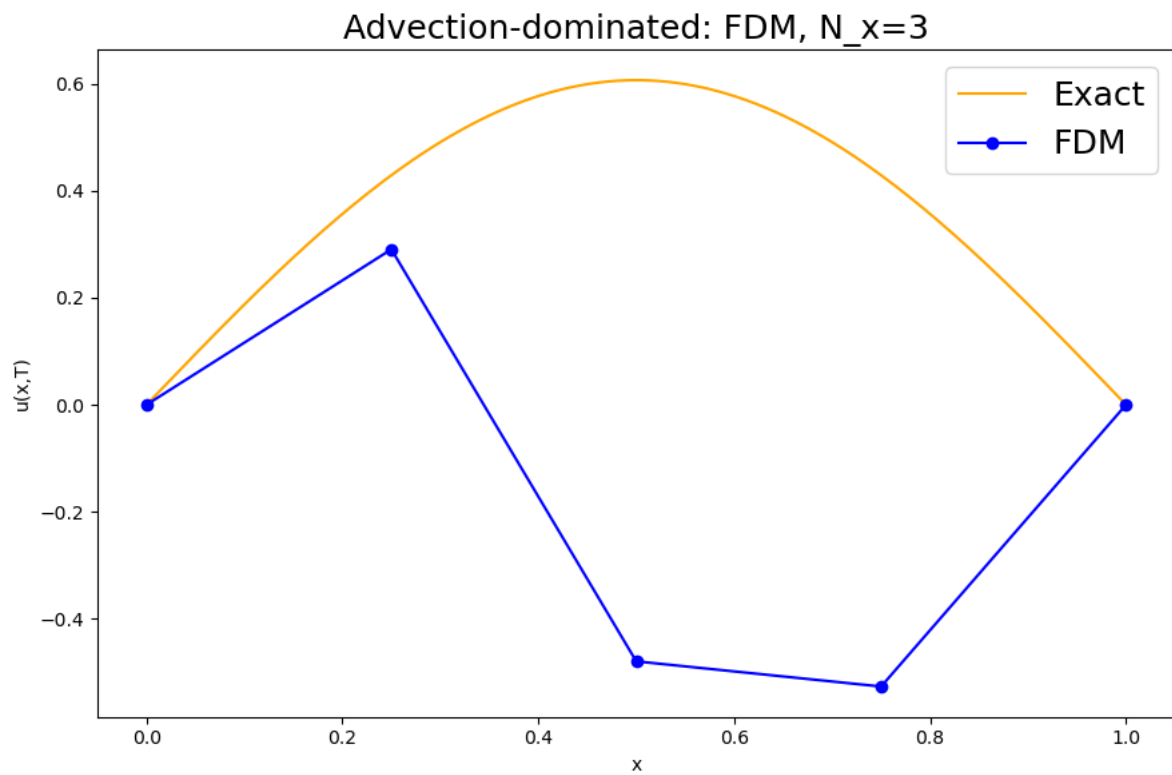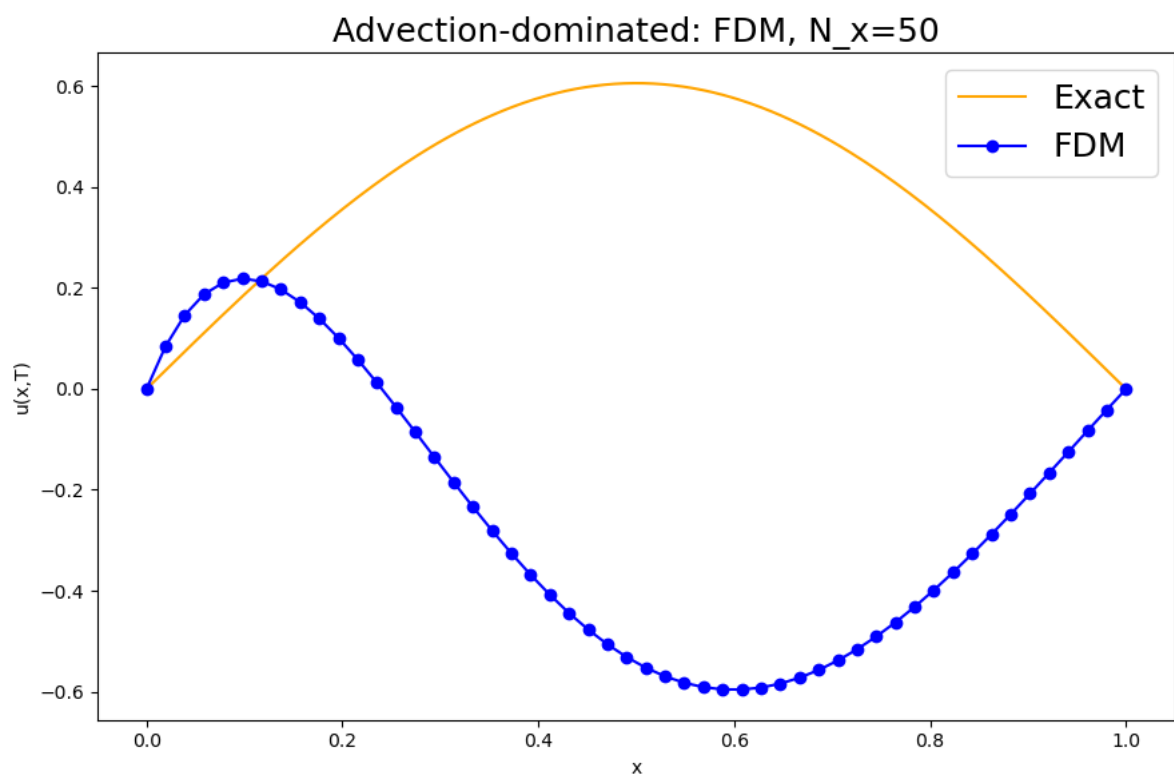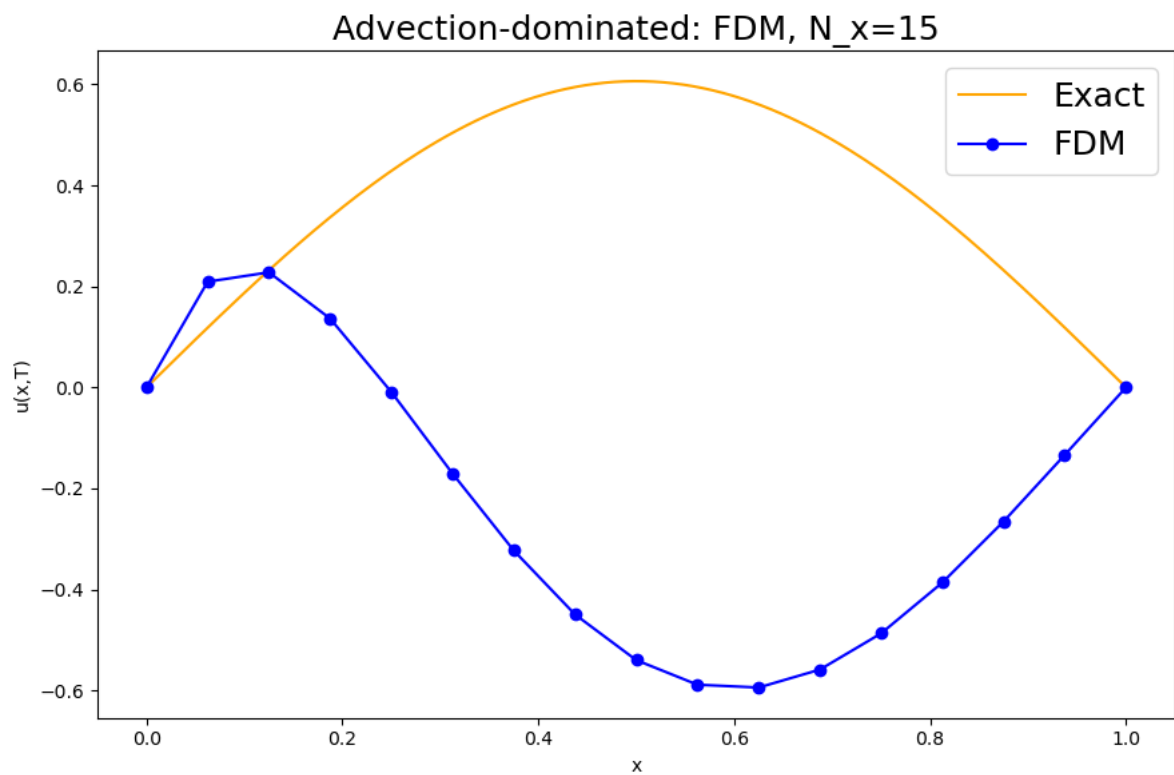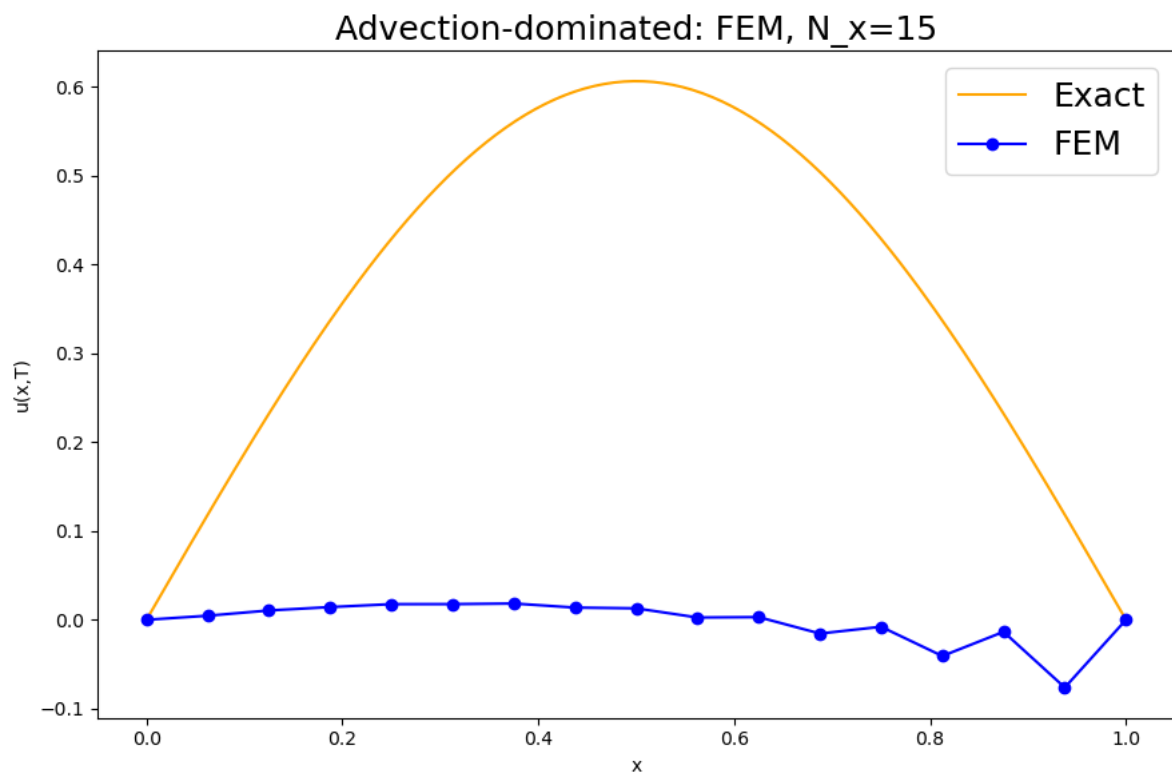

FDM, N_x=3

FDM, N_x=15

FDM, N_x=50

FEM, N_x=50
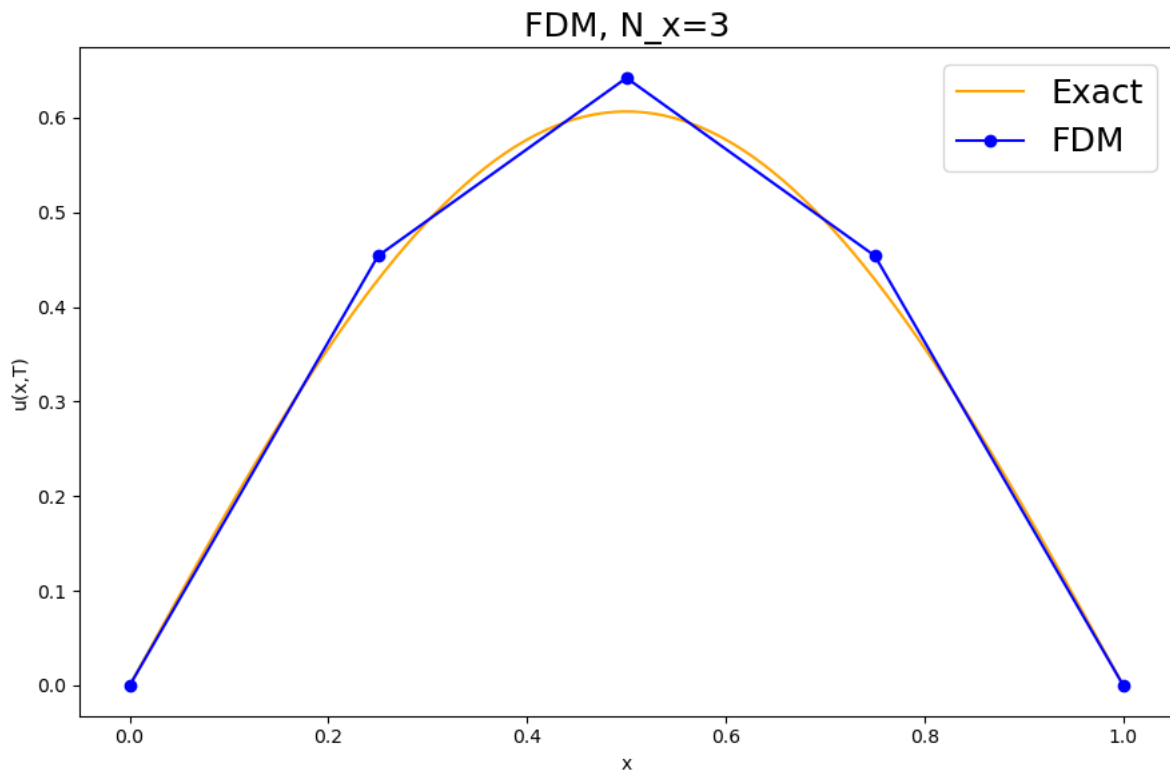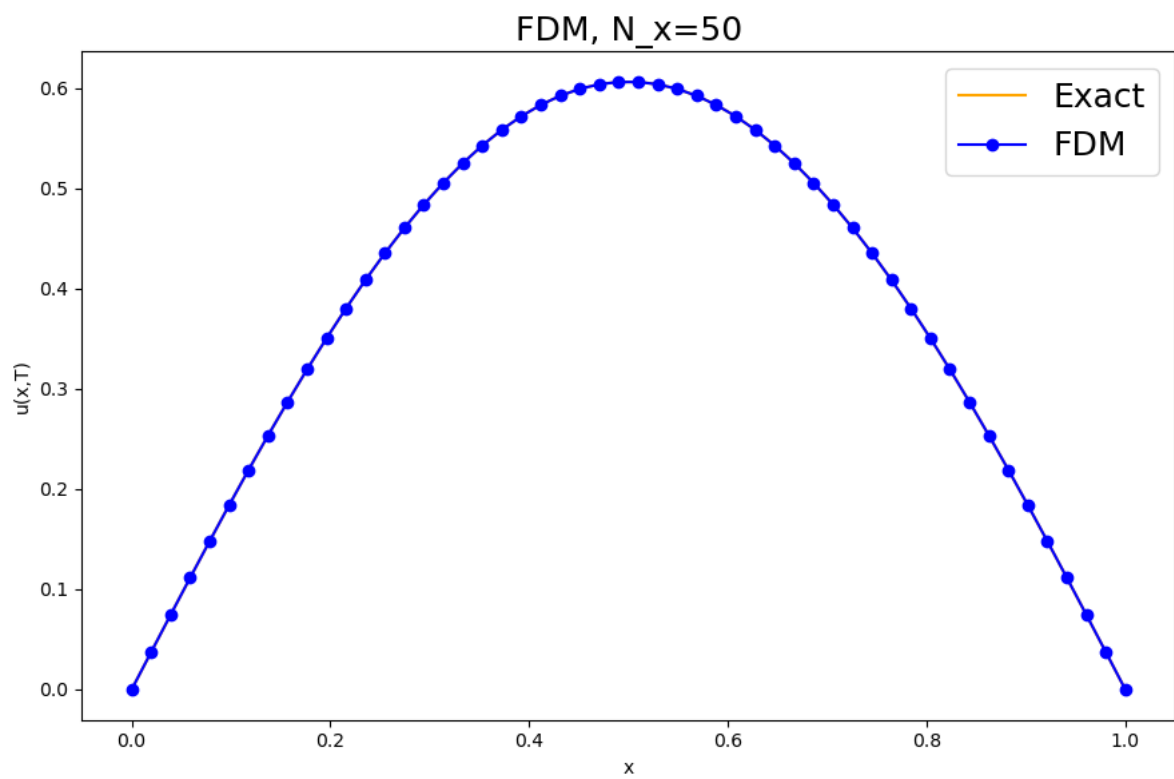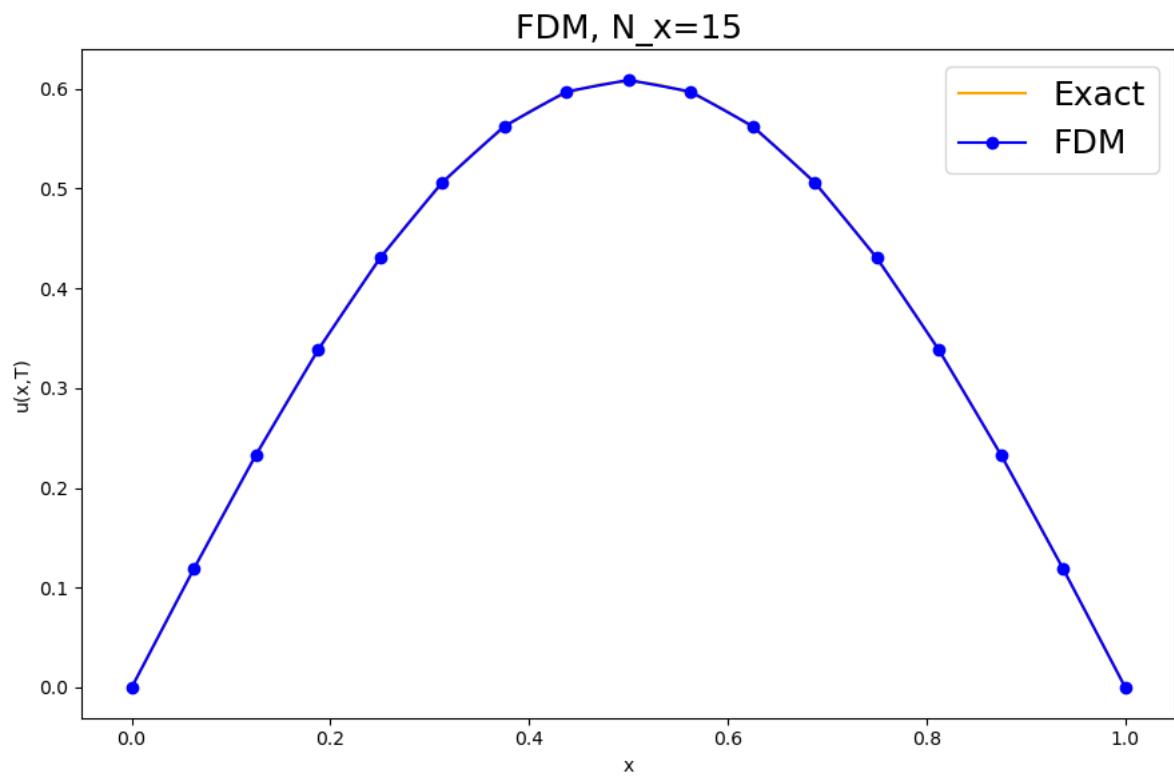
- The following plots represent the advection-dominated regime.

Advection-dominated: FDM, N_x=3

Advection-dominated: FDM, N_x=15

Advection-dominated: FDM, N_x=50

Advection-dominated: FEM, N_x=3

Advection-dominated: FEM, N_x=15

17

Advection-dominated: FEM, N_x=50
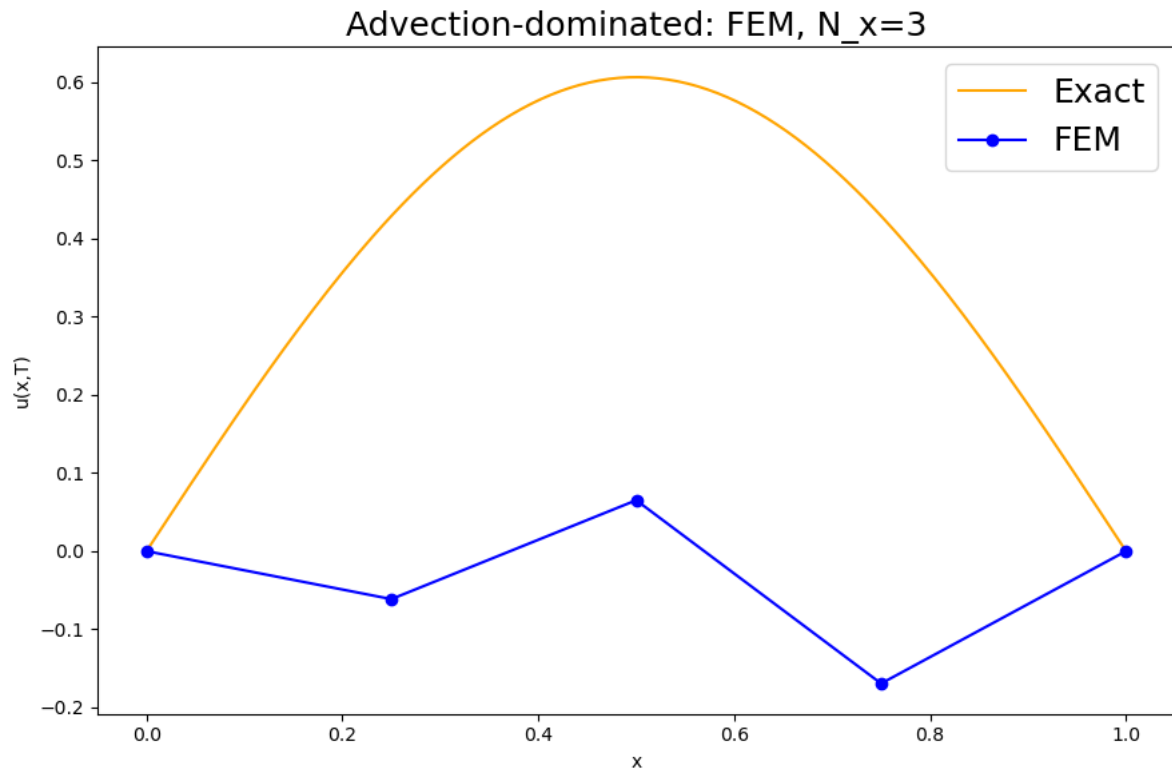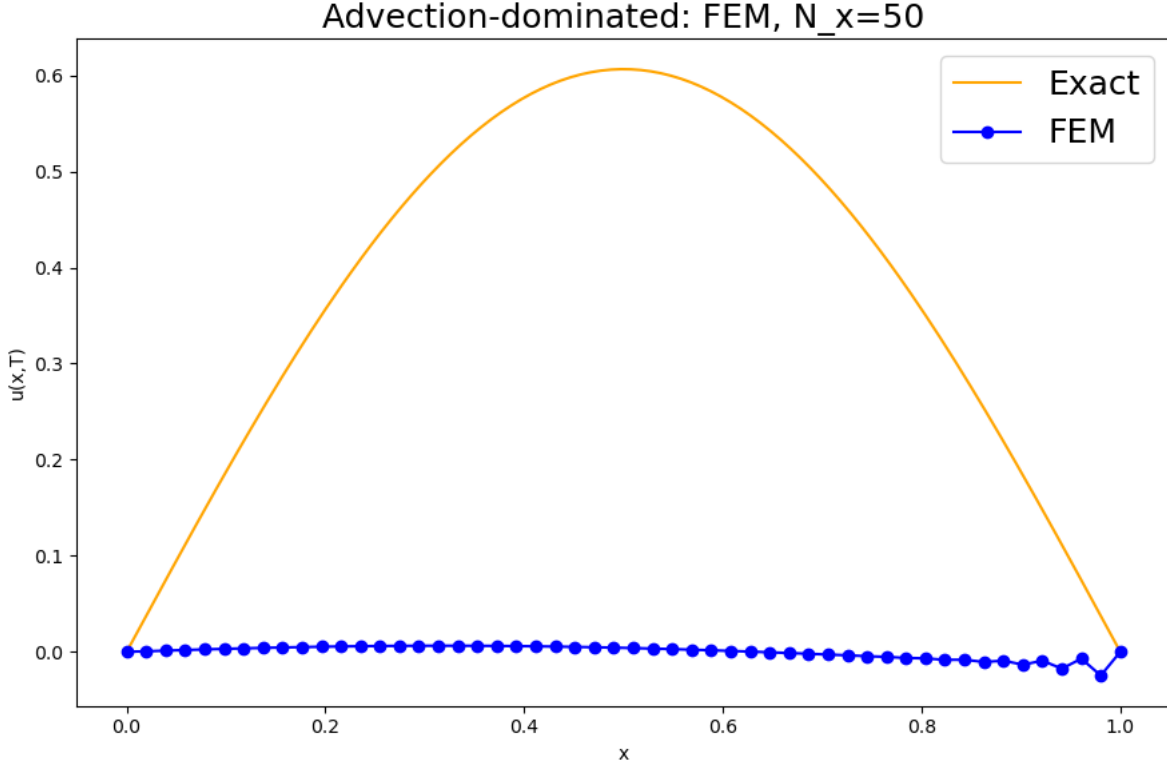
4. **Interpretation**

    (a) **Time-Step Assumption** $(\Delta t \sim \Delta x^2)$

        • From the pure-diffusion stability analysis (Lecture 21), the largest eigenvalue of the discrete Laplacian scales like

$$\lambda_{\max} \approx \frac{D}{\Delta x^2}.$$

        • To keep Crank–Nicolson's amplification factor

$$G(\lambda) = \frac{1 + \frac{\Delta t}{2}\lambda}{1 - \frac{\Delta t}{2}\lambda}$$

        safely bounded $(|G| \leq 1)$ and to drive the temporal truncation error to $\mathcal{O}(\Delta t^2)$, we choose

$$\Delta t = C\,\Delta x^2 \qquad (C < 1).$$

        • This makes the time-discretization error $\mathcal{O}(\Delta t^2) = \mathcal{O}(\Delta x^4)$, which is negligible compared to the spatial $\mathcal{O}(\Delta x^2)$ error. The result is a clean, slope-2 convergence on log–log plots that reflects purely spatial accuracy.

    (b) **Cell-Péclet Criterion** $(Pe_{\text{cell}} < 2 \text{ vs. } > 2)$

        • Define the local Péclet number in each cell as

$$Pe_{\text{cell}} = \frac{v\,\Delta x}{D}.$$

        • **Diffusion-dominated** $(Pe_{\text{cell}} < 2)$: central-difference stencils for u_x and the symmetric Galerkin form both remain stable and second-order accurate. Errors decay like Δx^2 because neither advective nor diffusive truncation terms dominate.

- **Advection-dominated** ($Pe_{\mathrm{cell}} > 2$): the central approximation of u_x admits dispersive errors and nonphysical oscillations; similarly, the symmetric FEM bilinear form lacks any upwind bias, so advective truncation terms overwhelm the diffusive Δx^2 behavior. On log–log error plots, the curves flatten or oscillate rather than follow the Δx^2 reference.

(c) **Physical Meaning of $\Delta t \sim \Delta x^2$**
- The characteristic time for diffusion to smooth variations over a length scale Δx is

$$t_{\mathrm{diff}} \approx \frac{\Delta x^2}{D}.$$

- By choosing Δt on the order of t_{diff}, each time-step resolves the physical process of mixing at the grid-scale.
- If $\Delta t \gg t_{\mathrm{diff}}$, the method "jumps" over key diffusive dynamics and error accumulates. If $\Delta t \ll t_{\mathrm{diff}}$, you waste computational effort resolving time-scales finer than necessary for spatial accuracy. The choice $\Delta t \sim t_{\mathrm{diff}}$ thus balances physical fidelity, stability, and computational efficiency.

4 Results and Discussion

In this section we present concise figures and commentary that directly address the four core questions posed in section 1.2. Each plot is accompanied by a short interpretation.

A. Boundary-Layer Thickness & Front Speed vs. Pe

For an initial Gaussian pulse on $[0, 1]$, pure convection–diffusion theory predicts:
- **Front speed** $s \approx v = Pe \cdot D/L$.
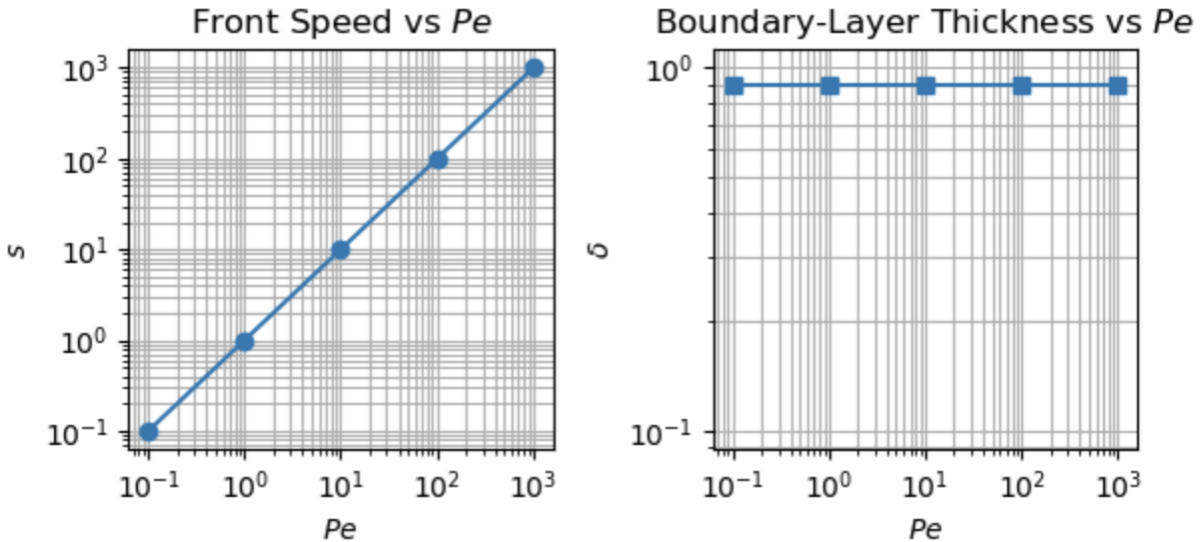- **Pulse width** (boundary-layer thickness)

$$\delta \sim 2\sqrt{D\,t_1},$$

independent of v.

In the following, we plot

$$s(Pe) = Pe, \qquad \delta(Pe) = 2\sqrt{D\,t_1},$$

with $D = 1$, $L = 1$, $t_1 = 0.2$. Log-log plots of front speed s and boundary-layer thickness δ versus Péclet number Pe confirm the expected scaling: $s \sim Pe$, $\delta \sim$ const.

B. Accuracy & Stability vs. Pe

In this test we fix the mesh at $N_x = 100$ (so $\Delta x = 1/101$) and choose $\Delta t = \Delta x$, then sweep

$$Pe = \frac{v\,\Delta x}{D} \in \{0.1,\ 1,\ 10,\ 100,\ 1000\}$$

to compare the discrete L^2 errors of:

- **FDM:** Crank–Nicolson in time with second-order central-difference in space.

- **FEM:** Crank–Nicolson in time with symmetric Galerkin piecewise-linear elements.

Using the manufactured solution $u_{\text{ex}}(x,t) = e^{-t}\sin(\pi x)$, we compute

$$E_{\text{FDM}} = \left(\Delta x \sum_{j=1}^{N_x} \left(u_j^N - u_{\text{ex}}(x_j, T) \right)^2 \right)^{1/2}, \quad E_{\text{FEM}} = \sqrt{(U^N - U_{\text{ex}})^T M (U^N - U_{\text{ex}})}.$$

We can make an observation that the central-difference FDM error remains low for $Pe \lesssim 2$ but then increases dramatically (e.g. from ~ 0.43 at $Pe = 1$ to > 2 at $Pe = 1000$), indicating loss of stability/accuracy in advection-dominated flows. In contrast, the symmetric Galerkin FEM error stays relatively bounded (around ~ 0.43–0.46) across the entire Pe range. This shows that, under these discretization settings, the undamped FDM scheme fails first as Pe_{cell} exceeds the stability threshold.
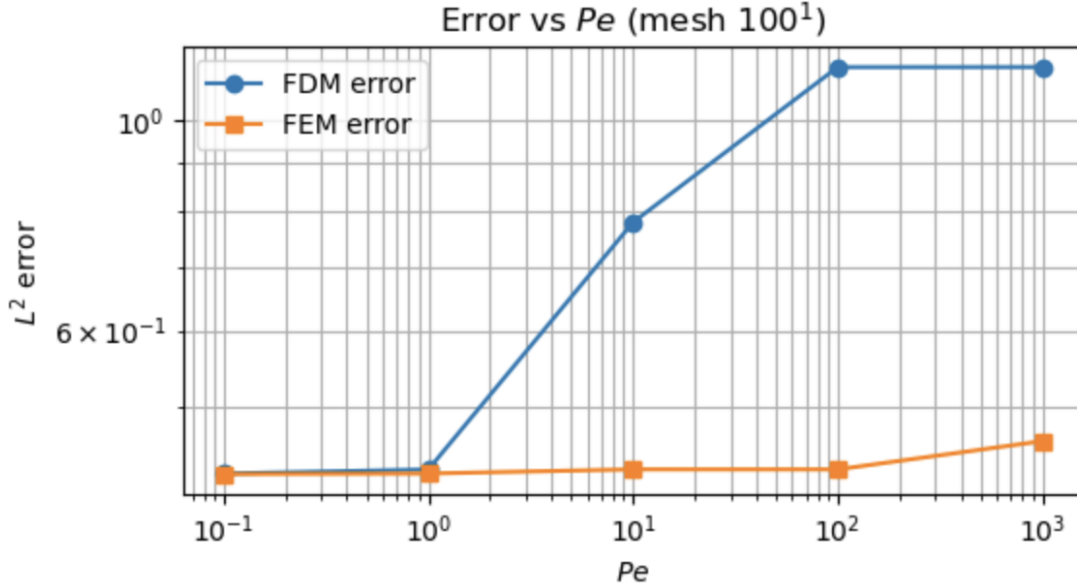
C. Cost–Accuracy Trade-Off

In this final test we evaluate both accuracy and computational cost for FDM and FEM at representative advection-dominated Péclet numbers

$$Pe \in \{10,\ 100,\ 1000\},$$

on a fixed grid with

$$\Delta x = \frac{1}{101}, \qquad \Delta t = \Delta x.$$

For each Pe, we record:

- **FDM error** $E_{\text{FDM}}(Pe)$ and time per solve using `time.perf_counter()`.

- **FEM error** $E_{\text{FEM}}(Pe)$ and time per solve.

The resulting table directly compares how the two schemes balance CPU time versus L^2 accuracy as advection dominance increases.

Pe	FDM error	FDM CPU	FEM error	FEM CPU
10	4.29×10^{-1}	0.008s	7.80×10^{-1}	0.007s
100	4.29×10^{-1}	0.008s	1.14×10^{0}	0.006s
1000	4.59×10^{-1}	0.005s	1.14×10^{0}	0.006s

5 Summary of Team Member Contributions

Rather than carve up the work into isolated chunks, our five-member team approached every rubric item problem definition, derivations, coding & convergence tests, and results interpretation—as a unified effort, with each of us participating fully at every stage. That said, several teammates stepped up with especially deep contributions: Kulvir enriched the IBVP motivation and refined the Gaussian pulse setup; Aadyanth lent exceptional rigor to the FDM/FEM consistency, stability derivations and built the reproducible GitHub repository; Aditi spearheaded the debugging, code optimization, and convergence-test implementation; Ram conceptualized and executed the Péclet-number sweep and visualization strategy; and Ayush seamlessly wove together the notebook organization, documentation, final report polishing. However, keep in mind that each member contributed to each other's tasks as needed. Each member invested roughly 20% of the effort, guaranteeing that all four core sections benefited from our collective creativity and these standout contributions.

6 Reproducibility

All code used to perform simulations, generate convergence plots, and visualize results is contained in a single well-organized Jupyter Notebook. This notebook includes modular implementations of both FDM and FEM solvers, as well as code for running accuracy tests, computing L^2 errors, and producing all plots shown in this report. The full notebook is uploaded onto GitHub at `https://github.com/AadyanthRao/AE370-Convection-Diffusion-IBVP/tree/main`, and is structured for clarity and reproducibility, making it easy to follow the numerical workflow end-to-end.

Acknowledgments